1998

Acoustic motion estimation and control for an unmanned underwater vehicle in a structured environmer

Caccia, M.; Casalino, G.; Cristi, R.; Veruggio, G.

Pergamon

M. Caccia, G. Casalino. R. Cristi, G. Veruggio, "Acoustic motion estimation and control for an unmanned underwater vehicle in a structured environment," Control Engineering Practice, v. 6, (1998) pp. 661-670.
http://hdl.handle.net/10945/56643

PERGAMON

Control Engineering Practice 6 (1998) 661–670

Acoustic motion estimation and control for an unmanned underwater vehicle in a structured environment

M. Caccia[a,*], G. Casalino[b], R. Cristi[c], G. Veruggio[a]

[a] *Consiglio Nazionale delle Ricerche, Istituto Automazione Navale, Via De Marini 6, 16149 Genova, Italy*
[b] *Dipartimento di Informatica, Sistemistica e Telematica, Università di Genova, Via Opera Pia, 13, Genova, Italy*
[c] *Department of Electrical and Computer Engineering, Naval Postgraduate School, Monterey, CA 93943, USA*

Received 1 December 1997

Abstract

The problem of identification and navigation, guidance and control in unmanned underwater vehicles (UUVs) is addressed in this paper. A task-function-based guidance system and an acoustic motion estimation module have been integrated with a conventional UUV autopilot within a two-layered hierarchical architecture for closed-loop control. Basic techniques to estimate the robot dynamics using the sensors mounted on the vehicle have been investigated. The proposed identification techniques and navigation, guidance and control (NGC) system have been tested on Roby2, a UUV developed at the Istituto Automazione Navale of the Italian C.N.R. The experimental set-up, as well as the modalities and results, are discussed.

Keywords: Underwater vehicles; navigation; guidance and control systems; motion-control systems; extended Kalman filter; identification; acoustics

1. Introduction

Theoretical and experimental results obtained from research into identification and navigation, guidance and control (NGC) in unmanned underwater vehicles (UUVs) are discussed in this paper. In this study, a guidance and control system based on a two-layered hierarchical architecture for closed-loop control (Casalino et al., 1996; Caccia et al., 1995) has been integrated with the conventional autopilot of Roby2, a testbed UUV developed at C.N.R.-I.A.N. The resulting system has been interfaced with an acoustic dynamic motion estimator designed for navigation in structured environments (Cristi et al., 1995; Cristi et al., 1996b), and has been tested in water.

Three key aspects of current research into operational UUVs have been investigated:

1.1. Identification of hydrodynamic derivatives

Marine science applications have driven the design and development of operational UUVs, characterized by interchangeable toolsleds able to carry equipment of various nature for different scientific missions (Newman and Stokes, 1994; Nokin, 1996; Veruggio et al., 1996). In this way, the vehicle dynamics changes at every mission, while applications require an enhancement in the performance of conventional UUV autopilots in terms of their precision and agility in maneuvering. In this frame, the development of low-cost methodologies for the identification of UUV hydrodynamic derivatives by means of the commercial sensor devices mounted on the vehicles has become fundamental. The numerical determination of a ship's hydrodynamic derivatives is traditionally carried out using towing-tank facilities such as rotating arms or planar motion mechanisms (Comstock, 1991). On the basis of these methods, the hydrodynamic coefficients are determined through tests that measure the forces and moments that act on a scale model of the vehicle in various motion conditions. Tests of this kind are generally rather time-consuming and expensive, and parameter estimation may be biased owing to scaling and data-reduction effects. These methods have largely been applied to torpedo-like and slender-body autonomous underwater vehicles (AUVs). One example is provided by tests carried out on a real vehicle, the MARIUS AUV

* Corresponding author. E-mail: max@ian.ge.cnr.it

0967-0661/98/$ – See front matter
PII S0967-0661(98)00057-4

(Ayela et al., 1995). With this kind of vehicle, the use of a complete coupled hydrodynamic model of a slender-body AUV makes it possible to design controllers that can manage maneuvers involving highly coupled dynamics (Healey and Lienard, 1993). Identifying an ROV through tests in a towing-tank can be fairly difficult and expensive, since the towing-bridge must be adapted to the actual vehicle and not to a scale model. For this reason, the feasibility of identifying ROV uncoupled motion with sufficient accuracy by means of simple in-water tests on a vehicle equipped with standard commercial sensors has been investigated. This approach should sensibly reduce costs, and should make it possible to ease identification tests in operational conditions that involve changes in the vehicle's hydrodynamic configuration (e.g., when different toolsleds are carried).

1.2. Low-speed UUV motion estimation

The performance of existing commercial devices (acoustic positioning systems, Doppler sonars, low-cost inertial units, etc.) is not adequate for UUV slow-motion estimation and localization (Ageev et al., 1995). Many optical and acoustic underwater vision systems are currently being investigated to perform high-precision motion estimation with respect to the operating environment. In the proximity of man-made structures, vehicle motion can be estimated in relation to the features detected by the vision systems, e.g. motion estimation on the basis of feature displacement with mono and stereo optical systems (Negahdaripour and Zhang, 1995), (Liu and Huang, 1986), (Maddalena et al., 1994). Land robotics results in vehicle planar motion estimation through range and bearing measurements using Kalman filtering techniques have been extended to underwater robotics for the case of structured environments sensed by time-of-flight sonar devices (Moran, 1994). This method permits high-precision motion estimation in the direction orthogonal to a tracked linear reflecting surface (Cristi et al., 1996a), (Stevens et al., 1996), and has been tested using a sonar mounted on the I.A.N.'s UUV prototype Roby2 (Cristi et al., 1996a).

1.3. Plan-and-move versus nested-loop Lyapunov-based guidance algorithm

Conventional approaches to vehicle motion control presuppose a clear distinction between the motion-planning phase and the subsequent motion-execution phase. On the basis of the so-called "backstepping procedure", which is outlined in (Kanella-Coupoulos and Kokotovich, 1991), a two-layered hierarchical architecture for closed-loop control which does not require any planning has been developed. This approach, which involves the definition of task-based operational variables, is suitable for handling distinctly different target approach manoeuvres, which require varying degrees of precision in motion control (Casalino et al., 1996). However, the approach adopts a task-independent inner control loop that implements a velocity servo loop, while traditional UUV autopilots performing autoheading, autodepth and autospeed work on position control rather than speed control. A simple transformation of velocity control into position control has been proposed in (Casalino et al., 1996), but until now this has not been tested on a UUV, where there is considerable uncertainty in motion estimation.

In this study, a 'Kalman-filter-based' acoustic navigation module and a 'two nested loops' guidance and control module have been combined to control the motion of the prototype UUV, Roby2. Some notes about hydrodynamic modeling and identification techniques for computing the hydrodynamic derivatives of a UUV by means of simple pool tests are presented in Section 2. Section 3 deals with acoustic motion estimation techniques based on a dynamic model of the vehicle and range and bearing data from sonar sweeps. The different tasks performed when approaching a target are discussed in Section 4, where the guidance algorithms based on Lyapunov control techniques are also presented.

A simple experiment was set up, in which Roby2 was to navigate in a swimming pool using a compass, a low-cost gyro and a pencil-beam profiling sonar. The resulting sensing system was only able to supply poor sensory information (10 Hz gyro and compass data and only 5 Hz range and bearing measurements), but, with the help of a dynamic model of the vehicle, this was sufficient to control the vehicle's motion between a series of waypoints on the horizontal plane. A thorough description of the test equipment and control architecture used in the NGC system, as well as the modalities and results, can be found in Section 5, which also presents the results of the tests for the identification of the planar motion hydrodynamic derivatives of Roby2.

The scope of this paper is limited to synchronous control and filtering modules, and coordination problems are only touched upon (i.e., logical and asynchronous aspects such as switching between different guidance tasks, multi-hypothesis arbiters for the association of sonar echoes with features of the environment, and environment model updating). Future steps in this direction, and possible system enhancements that should result from the application of new sensing devices, are discussed in the conclusions.

2. Hydrodynamic modeling and identification

The model used to describe the dynamics of ROVs is based on the motion equation of a rigid body in a fluid

medium. Since this is a standard model, it is not thoroughly discussed here, but relevant information can be found in (Yuh, 1990), (Fossen, 1994) and (Newman, 1977).

Two right-handed reference systems are needed: an inertial reference $\langle 0 \rangle$ with the z axis pointing downwards, and a non-inertial reference $\langle 1 \rangle$ fixed on the vehicle. The vehicle's orientation is specified by roll, pitch and yaw angles ϕ, θ, ψ, describing respectively rotations about the x_1, y_1, and z_1 axes, and giving origin to the rotation velocity ω of components p, q and r. The linear velocity components are surge u, sway v and heave w. v is the vector representing the vehicle's velocity in respect to the water in the non-inertial reference $\langle 1 \rangle$.

Newton's equation of motion for a rigid body in a fluid environment can be expressed in a 6-DOF vector notation. If the fluid is assumed to be still, the motion equation is:

$$(M + M_A)\frac{\mathrm{d}}{\mathrm{d}t}v + [C(v) + C_A(v)]v + D_1 v + D_2(v)v - gW\boldsymbol{k}'' - \boldsymbol{F}_C - \boldsymbol{F}_T = 0 \quad (1)$$

where $(M + M_A)$ is the sum of the inertial and added mass positive defined tensors, C is the Coriolis-centripetal tensor, and C_A its added mass equivalent. D_1 and D_2 are the linear and quadratic drag tensors, assumed diagonal.

Gravity acceleration is denoted by g, while $W\boldsymbol{k}''$ is a 6×6 force-moment vector, taking into account gravity and buoyancy effects; $\boldsymbol{k}''$ is a vector defined as: $\boldsymbol{k}'' = (-\sin\theta, \cos\theta \sin\varphi, \cos\theta \cos\varphi, -\sin\theta, \cos\theta \sin\varphi, \cos\theta \cos\varphi)^T$.

The generalized force vectors $\boldsymbol{F}_C$ and $\boldsymbol{F}_T$ are respectively related to cable and thruster effects.

To design conventional ROV control systems performing autodepth, autoheading and autospeed, a simplified version of Eq. (1) is generally considered. A typical example of a plane horizontal model is given by the following set of equations for surge, sway and yaw:

$$m_u\dot{u} = m_v vr - k_u u - k_{u|u|}u|u| + F_u \quad (2)$$

$$m_v\dot{v} = -m_u ur - k_v v - k_{v|v|}v|v| + F_v \quad (3)$$

$$I_r\ddot{r} = -(m_v - m_u)uv - k_r r - k_{r|r|}r|r| + T_r \quad (4)$$

where m_u, m_v, and I_r are the vehicle masses and moment of inertia (including added mass and inertia), while hydrodynamic damping is modeled as a linear and a quadratic term. F_u and F_v are the forces applied by the thrusters along the surge and sway directions, and T_r is the torque in the heave motion. This simplified model for the horizontal plane dynamics can be derived from Eq. (1), assuming M_A to be diagonal. Whatever the degree of approximation of the model, a major problem is the determination of the added mass and drag coefficients. In the case of operational UUVs, the development of methodologies to enable a fast identification is required in the operational field of the vehicle hydrodynamic derivatives, in order to increase the performance of the navigation data-filtering and automatic control systems. With this aim, consider the simplified dynamic equations (2–4), and note that the equations are nonlinear but that their structure is well suited for the identification of part of the parameters when particular dynamic or static conditions are met. For instance, if the system is excited only in the surge direction, maintaining the corresponding force/torque constant and the other equal to zero, Eq. (2) becomes:

$$-k_u u - k_{u|u|}u|u| + F_u = 0 \quad (5)$$

where the unknown parameters are the linear and quadratic drag coefficients, which can be determined using the measurement of the vehicle surge.

The estimation of the inertial coefficients is more difficult because the UUV must be accelerated. So far, particular inputs signals are required to excite all modes of the system, and these are usually called "persistently excited". Basically, the persistent excitation of the inputs guarantees the observability of the parameters, which is a fundamental prerequisite to apply any identification procedure. Many methods of identification are reported in the literature, and their performance varies from case to case. A classical approach consists of adopting a continuous-time least-square method (Caccia et al., 1997b) or an extended Kalman filter with state augmentation (Liu, 1993), so that the new state vector includes the parameters to be estimated. Recently, an approach based on the minimization of the fitting cost using a simulated annealing technique has been applied to the identification of the inertial and drag parameters of the yaw motion of Roby 2 (Caccia et al., 1997b).

3. Acoustic motion estimation

As discussed in (Cristi et al., 1996b), what is meant by the UUV world model is the robot's internal representation of its position, speed and operating site. In the case under examination, only the vehicle's planar motion at a constant depth is considered.

Vehicle position $\underline{p} = [x, y]^T$ is related to an earth-fixed reference frame, while vehicle speed $\underline{v} = [u, v]^T$ is represented in a vehicle-fixed reference frame (surge and sway).

According to Eqs (2) and (3), and assuming the absence of any current, the evolution in vehicle speed and position can be described by the following dynamic

model:

$$\begin{cases} x(k+1) = x(k) + \Delta t[u(k)\cos\psi_k - v(k)\sin\psi_k] \\ y(k+1) = y(k) + \Delta t[u(k)\sin\psi_k + v(k)\cos\psi_k] \\ u(k+1) = u(k) + \dfrac{\Delta t}{m_u}[m_v v(k) r_k - k_u u(k) \\ \qquad\qquad - k_{u|u|}\, u(k)|u(k)| + F_u(k)] \\ v(k+1) = v(k) + \dfrac{\Delta t}{m_v}[-m_u u(k) r_k - k_v v(k) \\ \qquad\qquad - k_{v|v|}\, v(k)|v(k)|] \end{cases} \tag{6}$$

where ψ_k and r_k are the vehicle heading and yaw rate estimated by a linear Kalman filter, and thrust F_u only appears in the surge equation because Roby2 has two longitudinal horizontal thrusters only. Test results have shown that a dynamic model of the vehicle has to be used to improve the precision of the estimate (Caccia et al., 1997a).

The operating site is represented as a collection of reflecting surfaces. A generic reflecting surface is described by the line representing the linear approximation of its intersection with the horizontal plane where the motion occurs:

$$\underline{a}_i^T \underline{x} + c_i = 0, \quad \text{with} \quad \underline{a}_i^T = [-\sin\alpha_i, -\cos\alpha_i], \tag{7}$$

where α_i is the orientation of the reflecting surface.

Let $\underline{b}(\beta, \psi)$ be the direction of the sonar beam in the earth-fixed reference frame, δr the sonar position in the vehicle-fixed reference frame and T the transformation matrix between the two different frames; the measurement equation is:

$$\underline{a}_i^T(\underline{p} + T\delta\underline{r} + \rho\underline{b}) + c_i = 0. \tag{8}$$

Writing it explicitly yields:

$$\rho(k) = \frac{-c_i - \underline{a}_i^T(\underline{p}(k) + T(\psi_k)\delta\underline{r})}{\underline{a}_i^T \underline{b}(\psi_k, \beta_k)}, \quad i = 1..n \tag{9}$$

which is a linear measurement equation in $\underline{p} = [x, y]^T$.

Therefore, the vehicle motion (position and speed) can be estimated by an extended Kalman filter.

As discussed in (Cristi et al., 1996b), successful motion estimation demands that the sonar echo be correctly associated with the surface that reflects it. The adopted arbiter associates a sonar measurement with the reflecting surface that minimizes $\varepsilon^T S^{-1}\varepsilon$, where ε is the innovation, i.e. the difference between the expected and the measured sonar ranges, and S the innovation covariance (Bar-Shalom and Fortmann, 1988). The generic m-th reflecting surface is regarded as a possible detected surface if $\varepsilon_m(k/k-1) S^{-1}_{k/k-1} \varepsilon_m(k/k-1) \leq$ Threshold. If no reflecting surface has been detected, the filter only updates the state on the basis of prediction.

Algorithm precision can be improved if a multi-hypothesis approach is introduced to manage uncertainty in sonar echo association.

4. Guidance loop

The design of the guidance loop is based on the general task-function approach described in (Samson et al., 1991). A candidate Lyapunov function of the task error, $V = V(\underline{e})$, is defined, and the control law is computed by setting $\dot{V} \leq 0$.

As discussed in (Casalino et al., 1996), the maneuvers that a UUV executes when heading towards a target can be grouped into three tasks:

- Long-range maneuvering (LRM): approaching the target area, regardless of vehicle orientation;
- Medium-range maneuvering (MRM): guiding the vehicle up to the target, with the required orientation;
- Short-range maneuvering (SRM): hovering above the target even in the presence of disturbances, which demands high-precision movement.

The following sub-sections discuss the guidance control laws proposed for the management of these tasks.

4.1. Long-range maneuvering

This task is performed by the vehicle when it is distant from the target, and its position does not need to be measured exactly. Vehicle heading, yaw rate and speed may be measured by a compass, a gyro and a Doppler velocimeter.

The goal of approaching the target is expressed by the task function $\underline{e} = [x\ y]^T$, and the following Lyapunov function is defined:

$$V(\underline{e}) = \frac{1}{2}\underline{e}^T\underline{e} = \frac{1}{2}(x^2 + y^2). \tag{10}$$

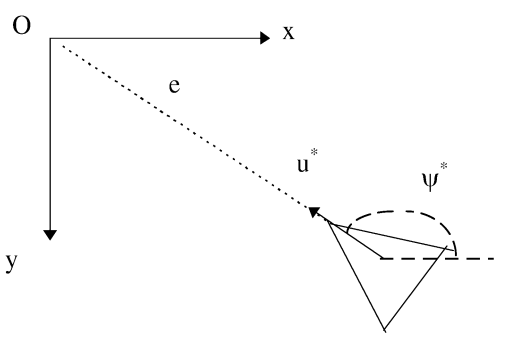

Fig. 1. Long-range maneuvering.

The control law is obtained by making the first time derivative of $V(x, y)$ negative:

$$\dot{V}(x, y) = (x\cos\psi + y\sin\psi)u + (y\cos\psi - x\sin\psi)v, \quad (11)$$

choosing:

$$\psi^* = a\tan2(-y, -x) \quad \text{(the vehicle heads for the target)} \quad (12)$$

and

$$u^* = -k(x\cos\psi^* + y\sin\psi^*), \quad k > 0. \quad (13)$$

$\dot{V}(x, y)$ is definite negative irrespective of the value of v and, in particular, for any u such that $u > 0$.

This guidance control law can easily be interfaced with conventional uncoupled UUV autopilots.

4.2. Medium-range maneuvering

Here, the vehicle is fairly close to the target and starts approaching it with the required orientation; its position can be established better than in the preceding case, one reason being that it is now moving inside an acoustic polygon (e.g., a long base line acoustic positioning system).

For the sake of simplicity, the desired orientation Ψ is assumed equal to zero.

This task is easily described by defining the task function $\underline{e} = [e\ \alpha\ \theta]^T$, which is chosen as in Fig. 2 and assumed to be completely measurable at any time. Variable e represents the distance error from the target frame; α measures the angle between advance orientation and the distance vector, while θ measures the angle between advance orientation and the x axis of the absolute tern $\langle O\rangle$, which coincides with the target frame.

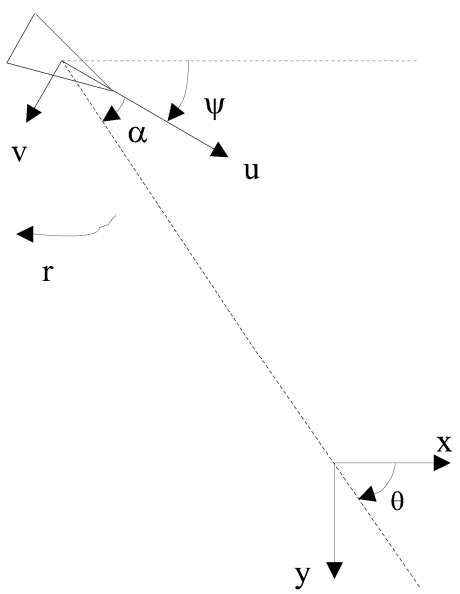

Fig. 2. Medium-range maneuvering.

The following equations are obtained:

$$\begin{cases} \dot{e} = -u\cos\alpha - v\sin\alpha \\ \dot{\theta} = \dfrac{u\sin\alpha}{e} - \dfrac{v\cos\alpha}{e} \\ \dot{\alpha} = -r + \dot{\theta} = -r + \dfrac{u\sin\alpha}{e} - \dfrac{v\cos\alpha}{e}. \end{cases} \quad (14)$$

It should be noted that this set of equations is valid only for distance errors e greater than zero; in the opposite case, both angles α and θ are simply found to be undefined quantities. This does not conflict with medium-range maneuvering where e is supposed to be other than 0.

The associated Lyapunov function has the form

$$V(\underline{e}) = V(e, \alpha, \theta) = \frac{1}{2}\lambda e^2 + \frac{1}{2}(\alpha^2 + h\theta^2). \quad (15)$$

The reference values for linear and angular velocities u^* and r^* in the external loop satisfy the following expressions (omitting here the calculation, see (Aicardi et al., 1995)):

$$u^* = \mu\, e\cos\alpha, \quad \mu > 0 \quad (16)$$

$$r^* = \mu\alpha + \gamma\frac{\cos\alpha\sin\alpha}{\alpha}(\alpha + h\theta), \quad \gamma > 0 \quad (17)$$

$$v^* = 0. \quad (18)$$

The last condition can be satisfied only in the case where the vehicle is equipped with transverse thrusters. Due to hydrodynamic damping and the use of some simple methods for improving algorithm performances (Caccia et al., 1995), even very small transverse thrusters are sufficient (if any are needed).

4.3. Short-range maneuvering

Short-range maneuvering is required when the vehicle hovers above the target. The area is often structured, and position and speed can be estimated by sonar (Cristi et al., 1996a; Stevens et al., 1996) and visual (Negahdaripour and Zhang, 1995) techniques. To hover above the target, the vehicle must be fully controllable, so it must be equipped with transverse thrusters as well as longitudinal ones.

The short-range maneuvering task function is $\underline{e} = [x\ y\ \psi]^T$, and the corresponding Lyapunov function is:

$$V(\underline{e}) = V(x, y, \psi) = \frac{1}{2}\lambda(x^2 + y^2) + \frac{1}{2}h\psi^2. \quad (19)$$

Differentiating (19) yields $\dot{V}$:

$$\dot{V} = \lambda[(x\cos\psi + y\sin\psi)u + (-x\sin\psi + y\cos\psi)v] + h\psi r. \quad (20)$$

Arbitrarily choosing:

$$u^* = -\mu_u(x\cos\psi + y\sin\psi), \quad \mu_u > 0 \tag{21}$$

$$v^* = -\mu_v(-x\sin\psi + y\cos\psi), \quad \mu_v > 0 \tag{22}$$

$$r^* = -\gamma\psi, \quad \gamma > 0, \tag{23}$$

$\dot{V}$ is negative definite and the vehicle heads towards the target, changing its initial orientation by rotating independently of the approach procedure.

4.4. Simulation results

In the following paragraph a simulated example of the sequence of the maneuvering tasks required to approach a target is presented for a fully controllable vehicle. In particular, the guidance system switches from long-range maneuvering to medium-range maneuvering when the distance from the vehicle to the target is 10 meters, while the short-range maneuvering task is scheduled when the vehicle is closer than 1 meter from the target. The resulting trajectory is shown in Fig. 3.

The long-range maneuvering task makes the vehicle head straight for the target: after a brief starting phase in which the vehicle points its fore end at the target, its distance e from the target decreases linearly (not exponentially because of thrust saturation) and the angle α goes to 0 (see Fig. 4).

When executing the medium-range maneuvering task, the vehicle approaches the target and lines up with it at the desired orientation, thus minimizing the task variables e and $(\alpha + \theta)$, $h = 1$ in (15). In this case, no transverse thruster is used to force v = 0; this creates a certain amount of vehicle drift that causes the quantity $(\alpha + \theta)$ to oscillate around 0 (see Fig. 5).

In short-range maneuvering, the distance $e = \sqrt{x^2 + y^2}$ from the target goes to zero exponentially; the small oscillation on the required orientation is typical of the PID heading controller implemented on Roby (see Fig. 6).

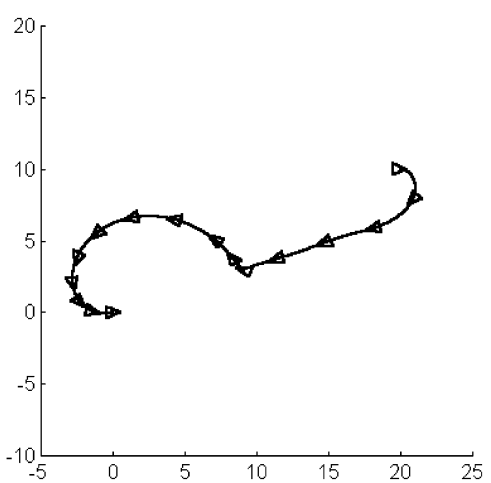

Fig. 3. Long-, medium- and short-range maneuvering trajectory.

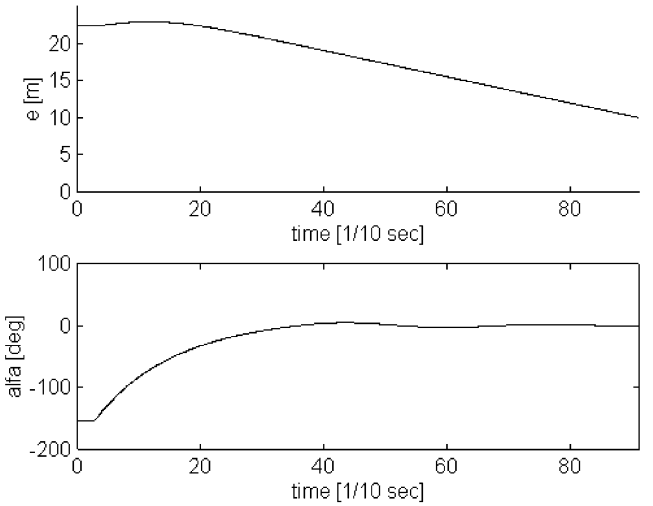

Fig. 4. Long-range maneuvering operational variables.

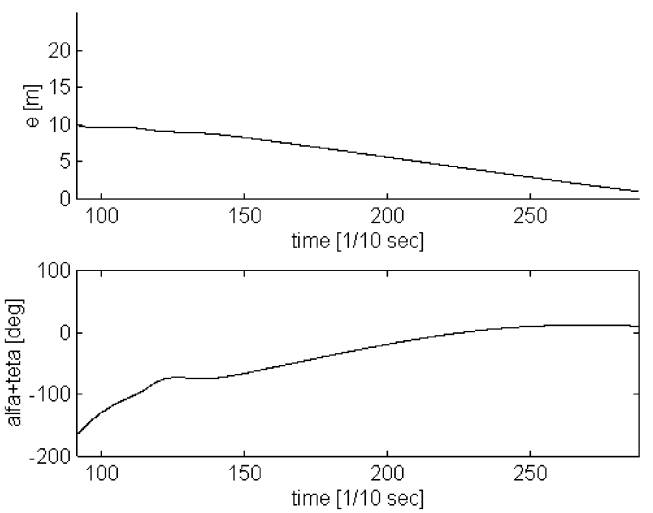

Fig. 5. Medium-range maneuvering operational variables.

5. Experimental set-up and results

The sonar used for testing is a Tritech ST1000 high-frequency (1.25 MHz) pencil-beam profiling sonar, whose head can rotate at increments of 0.9, 1.8 or 3.6 degrees. Due to the high frequency, the range is 50 meters in normal operating conditions. This frequency yields a 1.2 mm wavelength, a very narrow beam (about 1 degree conical) and high precision (not exceeding 1 cm) in range measurements. During the tests, the device was mounted on IAN's prototype vehicle Roby2, see Fig. 7. This tethered UUV is equipped with two horizontal and

two vertical thrusters, weighs about 250 Kg in air, is neutral in water and is stable in pitch and roll. It is controlled by an autopilot, which performs basic autoheading and autodepth functions. Heading and yaw rate measurements are taken by a compass and a low-cost gyro KVH-DGC100 (Everett, 1995), positioned at the top rear of the vehicle, where the disturbance caused by the electric thrusters is limited. The sonar therefore sees a blind spot generated by the compass cylinder when pointing backwards.

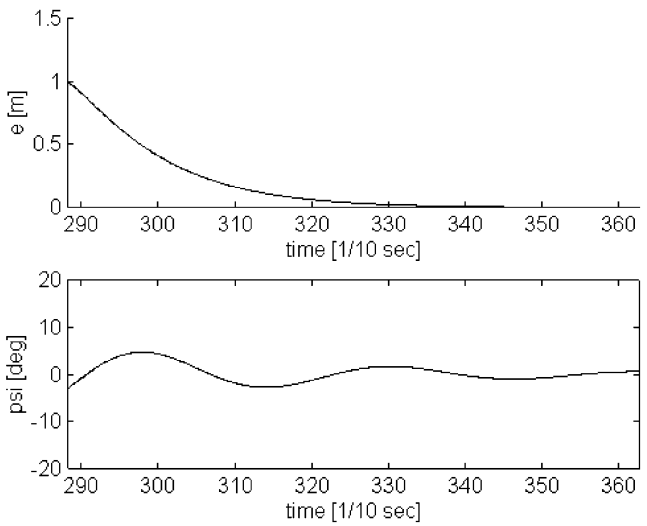

Fig. 6. Short-range maneuvering operational variables.

A number of tests have been performed in a high-diving pool measuring $33 \times 23 \times 5$ m. As the pool walls are highly reflective, the sonar is unable to detect them from a distance greater than 15 meters unless they are perpendicular to the beam.

At first, tests for the identification of the hydrodynamic coefficients have been carried out. In particular, Roby2 moved at constant longitudinal thrust orthogonally to a wall of the pool. Sonar range measurements allowed the steady-state surge reached by the vehicle to be evaluated. On the basis of the results reported in Table 1, the drag coefficients $k_u = 4.4303\ \mathrm{N\,s/m}$ and $k_{u|u|} = 344.9502\ \mathrm{N\,s^2/m^2}$ have been computed, applying a least-square procedure according to the model described by Eq. (5). The amount of thrust provided by the two horizontal thrusters was controlled using the thruster voltage/force relationship identified in a thrust tunnel at bollard conditions.

Exciting the vehicle with sequences of thrust steps of different amplitudes and time lengths, it has been possible to estimate the inertia of the vehicle in the surge direction by applying an extended Kalman filter with state augmentation algorithm to thrust and sonar range

Table 1
Steady-state Roby2 surge corresponding to constant thrust

F_u [N]	2.5	3.75	10	15	20	30	40
u [m/s]	0.06	0.08	0.16	0.21	0.24	0.29	0.33

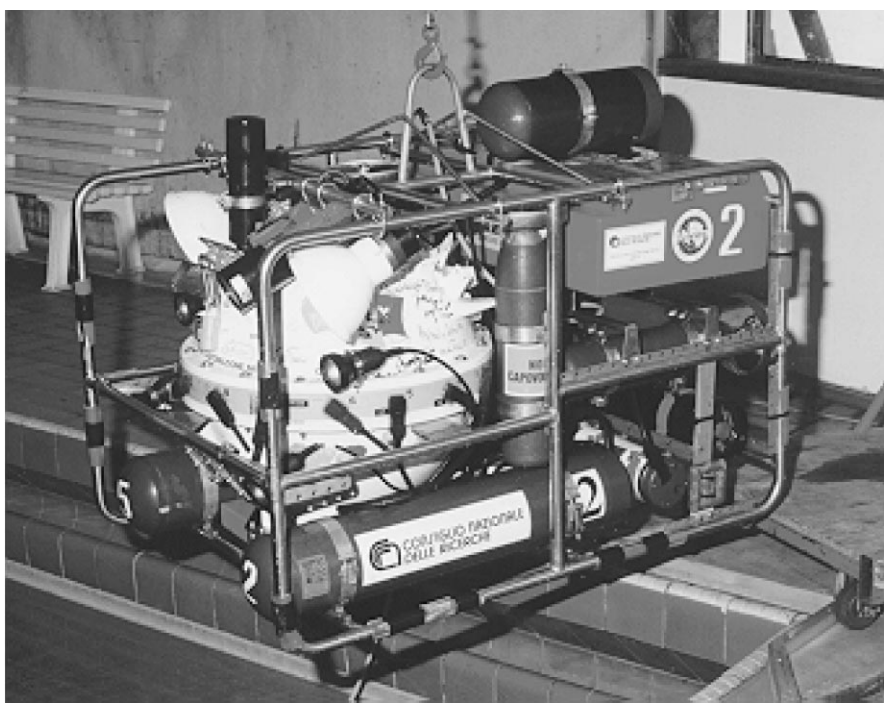

Fig. 7. Roby2: the digital gyro compass cylinder is visible on the top rear of the vehicle, while the profiling sonar is positioned on the top front of the vehicle.

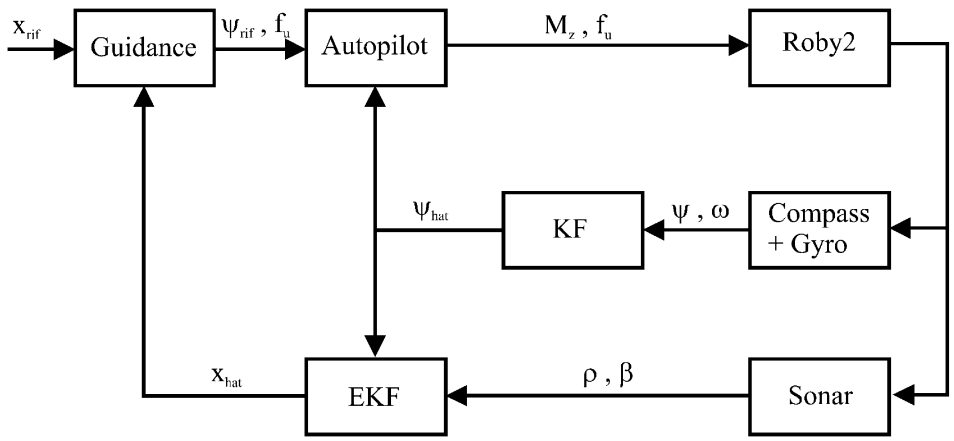

Fig. 8. Control architecture.

data. The computed mass m_u was about 350 Kg., i.e. the added mass was about 100 Kg.

During the tests of the NGC system, the sonar head rotated at 3.6-degree increments, and alternately scanned two perpendicular pool walls, sweeping a circular sector of approximately 120 degrees in the earth-fixed reference frame. Since the sonar acquisition frequency is 5 Hz, the vehicle motion was updated in the direction perpendicular to each pool wall approximately every 8 seconds, and therefore the position estimate was alternately uncertain in each of the two orthogonal directions, as reported in (Caccia et al., 1997a). The results provided by the motion-estimation module are therefore uncertain to a degree that is unacceptable in short- and medium-range maneuvering (particularly in linear speed estimation). In addition, the vehicle only has two horizontal thrusters, and its sway is not controllable. These technical constraints have suggested testing the integration of the motion-estimation module using a guidance system executing the long-range maneuvering task and the Roby2 autopilot, which provides autoheading and autodepth.

Since the first derivative of the LRM Lyapunov function is definite negative for any positive u, the guidance module simply controls the vehicle thrust in the surge direction in a way that it is proportional to the target distance ($f_u = ke$).

The resulting control architecture is described in Fig. 8. The autopilot's inner loop provides yaw estimation and force/torque computations while the guidance outer loop provides position estimation and computes the reference yaw and advance force for the autopilot.

Each test was organized into two phases: initialization, and navigation between way-points. At the beginning, the robot built a local map of the operating site, which is bordered by two roughly perpendicular walls. To do this, the vehicle stood virtually still (constant depth and orientation, no forward thrust) while its sonar swept the two pool walls; the orientation and distance of each wall was

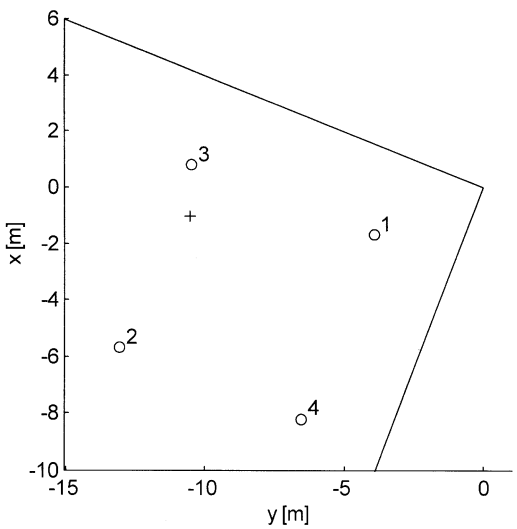

Fig. 9. Way-points and reconstructed environment map.

computed using the 'slope estimation' algorithm discussed in (Cristi et al., 1996a). The earth-fixed reference frame of the reconstructed local map was fixed at the intersection between the two walls, and the vehicle's initial position was computed on the basis of results obtained from the application of the 'slope algorithm' to the two walls.

Upon completion of the initialization phase, the vehicle moved between way-points while estimating its motion on the basis of the acoustic navigation algorithm described in Section 3. The two walls were alternately scanned by the sonar. Fig. 9 shows the reconstructed map and the way-points that were covered, in the order indicated by the numbers. When the vehicle was less than 1 meter from one target, the following way-point became the next target.

Roby2 covered the path three times: Fig. 10, 11 and 12 show the trajectory estimated on-line. It is possible to see that the course that the vehicle follows between

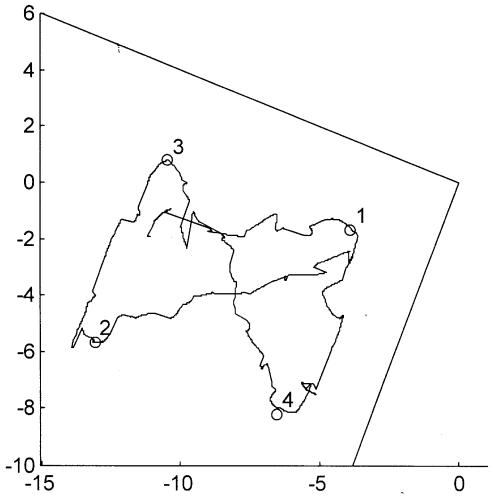

Fig. 10. On-line estimated trajectory (1st lap).

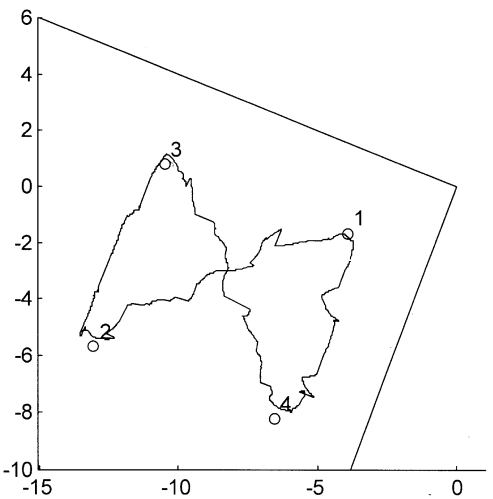

Fig. 11. On-line estimated trajectory (2nd lap).

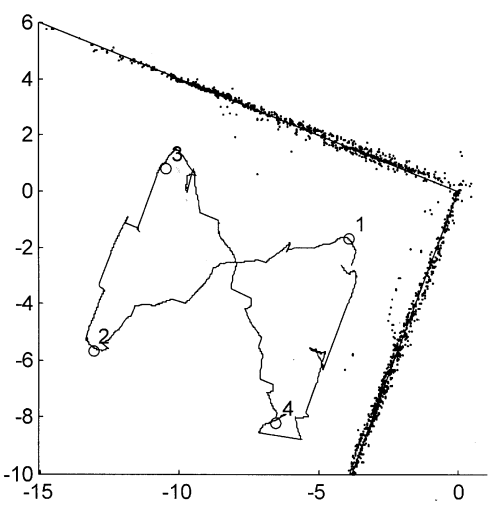

Fig. 12. On-line estimated trajectory (3rd lap) and sonar plots.

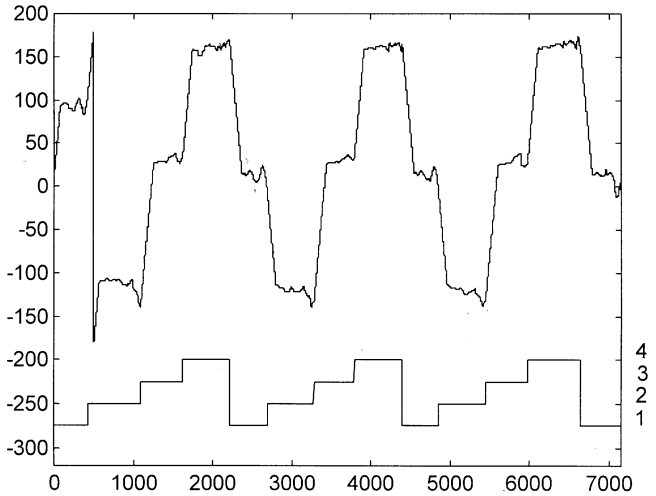

Fig. 13. Computed reference heading and way-point.

way-points 1 and 2 in the first lap differs from that followed in the second and third laps. In the first lap, the vehicle keeps to the left of the straight line linking points 1 and 2, while in the other two laps it keeps to the right; this behavior is typical of a Lyapunov-based guidance algorithm in the presence of different initial conditions. In addition (as shown in Fig. 13) where a temporal sequence of way-points is plotted, there are no time constraints on vehicle motion.

Fig. 12 also shows the sonar plots estimated on-line during the third lap, while the LRM computed reference heading is plotted in Fig. 13.

6. Conclusion

Pool tests carried out on Roby2 have shown that Lyapunov-based guidance systems produce satisfactory results in the presence of uncertainty in position estimation. Uncertainty is caused by the fact that the vehicle's position in a given direction is updated only every few seconds.

In view of this, a method that does not require any (re)planning when the position estimate is heavily corrected offers great advantages. If this algorithm is to be extended to medium- and short-range maneuvering, the performance of the motion estimator will have to be improved. Being EKF-based, the algorithm allows new sensors to be inserted quite easily: for instance, adding another pencil-beam profiling sonar will allow two perpendicular surfaces to be tracked simultaneously, achieving higher performance in motion estimation in both directions. In addition, the possibility of integrating these sensor devices with linear speed sensors (current meter, Doppler sonar), a motion reference unit and a monocular video system is being considered. The presence of a number of sensing devices will raise problems concerning

coordination, e.g. determining which sensors are needed at a certain time. As mentioned in the introduction, the coordination of navigation, guidance and control will be the focal point of future investigations.

Acknowledgments

The authors wish to thank all the staff of the Genoa City Council's Sports Authority for granting access to the municipal pool for testing. This work was partially funded by PNRA (Programma Nazionale di Ricerche in Antartide), Task 4a – Robotica e Telescienza in Ambiente Estremo. The authors thank Prof. Antonio Tiano, Dr. Giovanni Indiveri and Dr. Angelo Alessandri for their contribution in discussions about identification techniques, and their work in the determination of the yaw motion hydrodynamic derivatives of Roby2.

References

Ageev, M.D., Kasatkin, B.A., & Scherbatyuk, A. (1995). Positioning of an autonomous underwater vehicle. *Proc. of International Program Development in Undersea Robotics and Intelligent Control*, 15–17. Lisboa, Portugal.

Aicardi, M., Casalino, G., Bicchi, A., & Balestrino, A. (1995). Closed loop steering of unicycle vehicles via Lyapunov techniques. *IEEE Robotics and Automation Society Magazine*, *March*, 27–35.

Ayela, G., Bjerrum, A., Bruun, S., Pascoal, A., Pereira, F.L., Petzelt, C., & Pignon, J.P. (1995). Development of a self-organizing underwater vehicle – SOUV. *Second MAST Days and EUROMAR Market*, *2*, 1254–1269, Sorrento, Italy.

Bar-Shalom, Y., Fortmann, T.E. (1988). *Tracking and data association*. Academic Press.

Caccia, M., Carta Colombo, A., Casalino, G., Decia, M., & Veruggio, G. (1995). Closed-loop approach algorithm based on Lyapunov techniques for an autonomous underwater vehicle. *Proc. of the 3rd IFAC Workshop on Control Applications in Marine Systems*, 101–106, Trondheim, Norway.

Caccia, M., Cristi, R., & Veruggio, G. (1997a). Acoustic motion estimation in a structured environment for an unmanned underwater vehicle. *Proc. of SY.RO.CO'97*, *2*, 339–344, Nantes, France.

Caccia, M., Indiveri, G., Tiano, A., & Veruggio, G. (1997b). Experimental comparison of identification methods for an open-frame ROV. *4th IFAC Conference on Manoeuvring and Control of Marine Craft*, 1–6, Brijuni, Croatia.

Casalino, G., Cannata, G., &Caccia, M. (1996). Lyapunov based closed-loop motion control for UUVs. *Proc. of 3rd International Symposium on Methods and Models in Automation and Robotics*, *2*, 469–474, Miedzyzdroje, Poland.

Comstock, J.P. (1991). *Principles of Naval Architecture*. The Society of Naval Architects and Marine Engineers, New York.

Cristi, R., Caccia, M., Veruggio, G., & Healey, A.J. (1995). A sonar based approach to AUV localization. *Proc. of the 3rd IFAC Workshop on Control Applications in Marine Systems*, 291–298, Trondheim, Norway.

Cristi, R., Caccia, M., & Veruggio, G. (1996a). Motion estimation and modeling of the environment for underwater vehicles. *Proc. of 6th IARP in Underwater Robotics*, Toulon, France.

Cristi R., Caccia, M., & Veruggio, G. (1996b). Sonar environment modeling and motion estimation in UUV navigation. *Proc. 3rd International Symposium on Methods and Models in Automation and Robotics*, *2*, 481–488, Miedzyzdroje, Poland.

Everett, H.R. (1995). *Sensors for mobile robots – theory and application*. Wellesley, USA: A K Peters, Ltd.

Fossen, T.I. (1994). *Guidance and control of ocean vehicles*. John Wiley and Sons, UK.

Healey, A.J., & Lienard, D. (1993). Multivariable sliding mode control for autonomous diving and steering of unmanned underwater vehicles. *IEEE Journal of Ocean Engineering OE-18(3)*, 327–339.

Kanella-Coupoulos, I., & Kokotovich, P.V. (1991). Systematic design of adaptive controllers for feedback linearizable systems. *IEEE Transactions on Automatic Control*, AC-36.

Liu, G. (1993). Application of EKF technique to ship resistance measurement. *Automatica*, *29*(2), 275–283, 1993.

Liu, Y., & Huang, T.S. (1986). Estimation of rigid body motion using straight line correspondences. *Proc. International Conference Pattern Recognition*, Paris, France.

Maddalena, D., Prendin, W., & Zampato, M. (1994). Innovations on underwater stereoscopy: the new developments of the TV-Trackmeter. *Proc. Oceans 94 OSATES*, *2*, 150–156, Brest, France.

Moran, B.A. (1994). Underwater Shape Reconstruction in Two Dimensions. MIT Ph.D. Thesis. Cambridge, MA.

Negahdaripour, S., & Zhang, S. (1995). Determining the size and position of cylindrical objects from optical images in underwater environments. *Proc. of the 9th International Symposium on Unmanned Untethered Submersible Technology*, 232–242. Durham, USA.

Newman, J.B., & Stokes, D. (1994). Tiburon: Development of an ROV for ocean science research. *Proc. Oceans 94 OSATES*, *2*, 483–488, Brest, France.

Newman, J.N. (1977). *Marine hydrodynamics*. Cambridge, MA: MIT Press.

Nokin, M. (1996). ROV 6000 – a deep teleoperated system for scientific use. Proc. of 6th IARP in Underwater Robotics, Toulon, France.

Samson, C., Le Borgne, M., & Espiau, B. (1991). *Robot control*: *The task function approach*. Oxford Science Pubblications, Oxford Engineering Science Series, 22. Clarendon Press, Oxford, UK.

Stevens, A., Smith, R., & Probert, P. (1996). Developing a sonar-based underwater navigation system. *Proc. of 6th IARP in Underwater Robotics*, Toulon, France.

Veruggio, G., Caccia, M., & Bono, R. (1996). Romeo: a testbed vehicle for the virtual lab. *Proc. of 6th IARP in Underwater Robotics*, Toulon, France.

Yuh, J. (1990). Modeling and control of underwater robotic vehicles. *IEEE Transactions on Systems, Man and Cybernetics*, *20*(6), 1475–1483.